

Zeolite A coated $Zn_{1-x}Cu_xO$ MOS sensors for NO gas detection

Sezin Galioglu¹ · Irmak Karaduman² · Tuğba Çorlu² · Burcu Akata^{1,3} ·
Memet Ali Yıldırım⁴ · Aytunç Ateş⁵ · Selim Acar¹

Received: 20 September 2017 / Accepted: 11 October 2017 / Published online: 25 October 2017
© Springer Science+Business Media, LLC 2017

Abstract In the current study, a novel and highly sensitive gas sensing material for the detection of NO gas was reported. Copper doped zinc oxide nanostructures ($Zn_{1-x}Cu_xO$, where $x=0.25$ steps) were grown as a semi-conducting sensor material by using Successive Ionic Layer Adsorption and Reaction (SILAR) method. The structural, morphological and optical properties of nanostructures were investigated by X-Ray Diffractometer (XRD), Scanning Electron Microscope (SEM) and UV–visible spectrometer. NO gas sensing measurements were carried out as a function of temperature and gas concentrations. The sensors exhibited acceptable responses towards 50 ppb NO gas at operating temperature of 55 °C. The sensors were optimized and the maximum response of 8% was obtained for the $Zn_{0.75}Cu_{0.25}O$ sensor. To increase sensor selectivity, zeolite A (LTA) microporous film, used as a filter, was coated on the optimized $Zn_{0.75}Cu_{0.25}O$ sensor by using secondary

growth method. zeolite A coated $Zn_{0.75}Cu_{0.25}O$ sensor exhibited both high selectivity and high response towards NO gas. The detection limit of the zeolite coated $Zn_{0.75}Cu_{0.25}O$ sensor was shifted to 20 ppb for NO gas at operating temperature of 25 °C.

1 Introduction

Recently, semiconducting metal oxide (MOS) gas sensors have attracted considerable attention because of their many advantages over traditional chemical analysis methods; these advantages include fast response, high sensitivity, small dimensions, ease of use, portability, simple design, simplicity of fabrication, real-time detection, low detection limits, low cost, and low power consumption [1, 2]. Among them, ZnO is the technologically important semiconducting material used as a sensing material due to its low cost, long-life, thermal and chemical stability and simple fabrication process [2].

Successful development of ZnO based gas sensors for commercialization requires achieving three “S”: sensitivity, selectivity, and stability [3]. Among them, stability is considered as the most important requirement for commercial devices with other properties remaining acceptable. Sensitivity is usually improved by doping noble catalyst particles and annealing processes. It is closely related to the detection limit of the sensor, which at present is as low as several ppm for the commercially gas sensor. Li et al. demonstrated that Ce-doping was increased sensing properties of ZnO microspheres sensors which operated at low temperature [4]. They reported that the Ce doped ZnO microspheres exhibited the highest sensitivity with rapid response and recovery times compared to pure one [4]. Hjiri et al. reported the Al-doped ZnO sensorexhibiting

Electronic supplementary material The online version of this article (doi:10.1007/s10854-017-8042-8) contains supplementary material, which is available to authorized users.

✉ Irmak Karaduman
irmak.karaduman06@gmail.com

- ¹ Department of Micro and Nanotechnology, Middle East Technical University, Ankara, Turkey
- ² Department of Physics, Science Faculty, Gazi University, Ankara, Turkey
- ³ Central Laboratory, Middle East Technical University, Ankara, Turkey
- ⁴ Department of Electric Electronics Engineering, Engineering Faculty, Erzincan University, Erzincan, Turkey
- ⁵ Department of Material Engineering, Engineering and Natural Sciences Faculty, Yıldırım Beyazıt University, Ankara, Turkey

a higher response than the pure ZnO and allowing the detection of CO at sub-ppm concentrations in the air [5]. Gómez-Pozos et al. showed that the using of Cu as a dopant in ZnO films led to an excellent catalytic effect and enhanced the response of the sensor. It was shown that Cu doping into the ZnO improved the gas sensitivity due to localized impurity levels created in ZnO lattice by Cu doping [6]. Chow et al. demonstrated that Cu doping into the ZnO sensors enhanced the sensitivity, showed faster response time, good selectivity and low power consumption compared to undoped ZnO sensors [7].

In terms of selectivity, the ability of selective detection in the presence of interfering gas mixture is very difficult. The main problem of MOS sensors is their inherent lack of selectivity [8–10]. To overcome the lack of selectivity in MOS, several strategies have been proposed: (i) Choosing the optimum operating temperature where it shows the maximum sensitivity toward the target gas [11]; (ii) Growth the sensing material by careful control of the growth and annealing treatment process or incorporating special promoters or noble metal particles which selectively enhance surface reaction with the target gas; (iii) To provide maximum selectivity, changing the design of the sensor structure that involves the design of the electrode, the thickness of sensing layer, and the size and shape of the sensor; (iv) Using a physical [12] or a chemical filter [13] over the sensing element. Adsorbent barriers can be placed between the sensor surface and the atmosphere as a filter, which adsorbs various interfering gases [14]. Zeolite filters are very convenient to prompt selectivity and sensitivity due to their physicochemical properties. The incorporation of zeolite materials into MOS gas-sensing systems has mostly been in the form of layers on top of the control material, referred to as over layers or coatings [15]. The recent preparation of zeolites with enhanced accessibility to their micropores by reduction of zeolite particle sizes going from micron to nanometer-sized dimensions affords enhanced physical properties such as increased specific surface area and decreased diffusion path lengths [16]. This offers additional advantages towards the extraordinary performance of zeolite materials for catalytic, adsorption, membrane and sensing applications [16].

The purpose of study is to produce sensor materials with high sensitivity that can provide gas selectivity at low gas concentrations. In the current study, $Zn_{1-x}Cu_xO$ (where, $x=0, 0.25, 0.50, 0.75$, and 1) nanostructures were grown by using SILAR method and their NO gas sensing properties were systematically investigated. NO gas sensing measurements were carried out as a function of temperature and gas concentrations. The prepared sensors were optimized according to gas sensing measurements in terms of sensitivity, repeatability, stability, response and recovery times. To increase sensor selectivity, zeolite A (LTA) film, used as a filter in between the sensor and the gaseous atmosphere,

was coated on the optimized $Zn_{0.75}Cu_{0.25}O$ sensor by using secondary growth method. To the best of our knowledge, this is the first report about NO gas sensing properties of intergrown zeolite A coated $Zn_{1-x}Cu_xO$ MOS sensor.

2 Experimental

2.1 Growth of the $Zn_{1-x}Cu_xO$ ($x=0, 0.25, 0.50, 0.75$, and 1) nanostructures

The interdigitated gold electrodes were coated on a glass substrate by e-beam. Then, $Zn_{1-x}Cu_xO$ (where, $x=0, 0.25, 0.50, 0.75, 1$) nanostructures were grown on electrodes at room temperature by using Successive Ionic Layer Adsorption and Reaction (SILAR) method [17]. The SILAR method resembles chemical bath deposition but deposition control of the growth is easier since the precursors for the cation and anion constituents of the nanostructures are in different vessels. The growth of nanostructures in the SILAR method occurs only heterogeneously on the solid–solution interface due to the intermediate rinsing step between the cation and anion immersions. The equipment for the SILAR method can be very simple and inexpensive due to the ambient growth conditions used.

To grow $Zn_{1-x}Cu_xO$ nanostructures, aqueous zinc–ammonia complex ions ($[Zn(NH_3)_4]^{2+}$) and aqueous copper–ammonia complex ions ($[Cu(NH_3)_4]^{2+}$) were chosen for the cation precursors, in which trace metals basis of $ZnCl_2$ (99.9%, Sigma-Aldrich) of 0.1 M, $CuCl_2$ (99.9%, Sigma-Aldrich) of 0.1 M as sources for Zn, Cu and aqueous ammonia solution (NH_3 -28%, Sigma-Aldrich) were used. Deionized water was used as a solvent. The molar ratio 1:10 of Zn-Cu: NH_3 was obtained as a result of several experiments [18, 19]. One SILAR cycle involves the four following steps: 1) immersing the substrate in the Cu–Zn species for 15 s (ZnO), 18 s (CZO) and 18 s (CuO) to create a thin liquid layer containing Zn–Cu ammonia complex ions on the substrate; 2) immersing immediately the withdrawn substrates in hot water ($\sim 90^\circ C$) for 7 s to form a $Zn_{1-x}Cu_xO$ layer; 3) drying the substrate in the air for 60 s and 4) rinsing the substrate in a separate beaker for 30 s to remove large and loosely bonded Zn–Cu particles. Thus, one SILAR cycle of $Zn_{1-x}Cu_xO$ nanostructures growth was completed. The obtained $[Zn(NH_3)_4]^{2+}$ and $[Cu(NH_3)_4]^{2+}$ complexes were mixed in appropriate proportions according to the composition for ZnO (S0), $Zn_{0.75}Cu_{0.25}O$ (S1), $Zn_{0.50}Cu_{0.50}O$ (S2), $Zn_{0.25}Cu_{0.75}O$ (S3), and CuO (S4) nanostructures. $Zn_{1-x}Cu_xO$ nanostructures were grown by repeating 40 SILAR cycles. The nanostructures were annealed in a nitrogen atmosphere ($300^\circ C$ for 13 min) and characteristic parameters of the nanostructures were investigated.

2.2 Preparation of zeolite A (LTA) films on $\text{Zn}_{0.75}\text{Cu}_{0.25}\text{O}$ sensors

The zeolite A film preparation procedure consisted of two steps: seed layer formation followed by growth of these seed crystals. In the first step, zeolite A crystals were deposited by spin coating at 5000 rpm for 30 s on $\text{Zn}_{0.75}\text{Cu}_{0.25}\text{O}$ sensors (10 mm × 25 mm) using an ethanol suspension containing 5 wt% of 100 nm-sized zeolites A crystal. Seed crystals were synthesized hydrothermally by using the molar composition of $11.25\text{SiO}_2:1.8\text{Al}_2\text{O}_3:13.4(\text{TMA})_2\text{O}:0.6\text{Na}_2\text{O}:700\text{H}_2\text{O}$ [20]. In this preparation, tetramethylammonium hydroxide (25 wt% TMAOH, Aldrich) and aluminum isopropoxide (98+ %, Aldrich) were dissolved in ultrapure deionized water and stirred for 1 h at room temperature. After dissolving these components, tetraethyl orthosilicate (99+ % TEOS, Acros) and sodium hydroxide (97% NaOH, J.T. Baker) were added and viscous gel stirred for 15 h at room temperature. The mixture was transferred into 60 mL high-density polyethylene (HDPE) bottle. The static synthesis was carried out for 8 h at 100 °C; the products were cooled to room temperature, centrifuged, washed with deionized water, and dried overnight in ambient air at ~70 °C.

The seeded sensors were heat-treated in ambient air (heating from 30 to 350 °C at 5 °C/min, isothermal heating at 350 °C for 9 h, and convective cooling to 30 °C). In the second step of zeolite A film preparation, the seed crystals deposited $\text{Zn}_{0.75}\text{Cu}_{0.25}\text{O}$ sensors were grown by using molar composition of $0.12\text{NaO}_2:5\text{SiO}_2:0.72\text{Al}_2\text{O}_3:5.8(\text{TM A})_2\text{O}:250\text{H}_2\text{O}$ [20]. In this preparation, tetramethylammonium hydroxide (25 wt% TMAOH, Aldrich) and aluminum isopropoxide (98+ %, Aldrich) were dissolved in ultrapure deionized water and stirred for 1 h at room temperature. After dissolving these components, silica sol (HS-40 wt%, Aldrich) and sodium hydroxide (97% NaOH, J.T. Baker) were added. The resulting viscous gel was stirred for 24 h at room temperature to form secondary growth mixture. The $\text{Zn}_{0.75}\text{Cu}_{0.25}\text{O}$ sensors with seed layers facing downwards were diagonally placed in the conic centrifugation tubes. The substrates were completely submerged in the growth mixture. After 9 h static hydrothermal treatment at 100 °C, the contents of the centrifugation tube were cooled to room temperature in cold water. Some phase separation/settling in the growth mixture was observed after hydrothermal treatment; however, the white structured fluid still covered the substrates. The zeolite A films supported on the $\text{Zn}_{0.75}\text{Cu}_{0.25}\text{O}$ sensors were removed from the growth mixture, thoroughly rinsed with 1 L deionized water, immediately air-dried using an air gun, and left overnight to dry at room temperature in ambient air.

2.3 Materials characterization

To investigate structural, morphological and optical properties of the $\text{Zn}_{1-x}\text{Cu}_x\text{O}$ nanostructures, XRD, SEM and optical absorption measurements were used. For structural and morphological studies, the Panalytical Empyrean X-Ray Diffractometer (using $\text{Cu K}\alpha$ $\lambda = 1.5405$ Å radiation) and the FEI Quanta FEG 450 model Scanning Electron Microscope were used, respectively. For the optical characterization, the Perkin-Elmer UV/VIS Lambda 2S Spectrometer was used. After that, morphological properties of the zeolite A coated sensor was examined by Field Emission Scanning Electron Microscope (FE-SEM, FEI Quanta 400). Phase identification of zeolite A coated sensor was done by the Rigaku-Ultima IV X-ray powder diffraction (XRD) by using thin film attachment with grazing angle of 0.3°.

2.4 Gas sensing measurements

The gas sensing performance of the sensors was tested using a special computer-controlled measurement system described in detail our previous studies [21, 22]. Produced sensors were evaluated by measuring the resistance change at various gas concentrations from 50 ppb to 25 ppm. The gas concentration in the test chamber was controlled by mass flow controllers (MKS Series). A LakeShore 325 temperature controller with platinum RTDs was used to maintain a constant temperature. The current of the sensor was continuously monitored with a computer-controlled system using the Keithley 2400 Source Meter and the data was collected in real-time using a computer with corresponding data acquisition hardware and software. The relative humidity was kept constant 25% and monitored by a Honeywell HIH-4000 humidity sensor. The sensor response was calculated using the following equation [22];

$$S (\%) = \left(\frac{R_g - R_a}{R_a} \right) \times 100 \quad (1)$$

where, R_a and R_g are the resistance in dry air and resistance upon exposure to the target gas in dry air, respectively.

3 Result and discussion

3.1 Structural, morphological, and optical analyses

Figure 1 shows the XRD patterns of the $\text{Zn}_{1-x}\text{Cu}_x\text{O}$ nanostructures. As seen in Fig. 1, all the nanostructures had polycrystalline nature and well-defined peaks belonging to ZnO and CuO nanostructures. The pure ZnO nanostructure ($x = 0$) had hexagonal wurtzite phase with (100), (002),

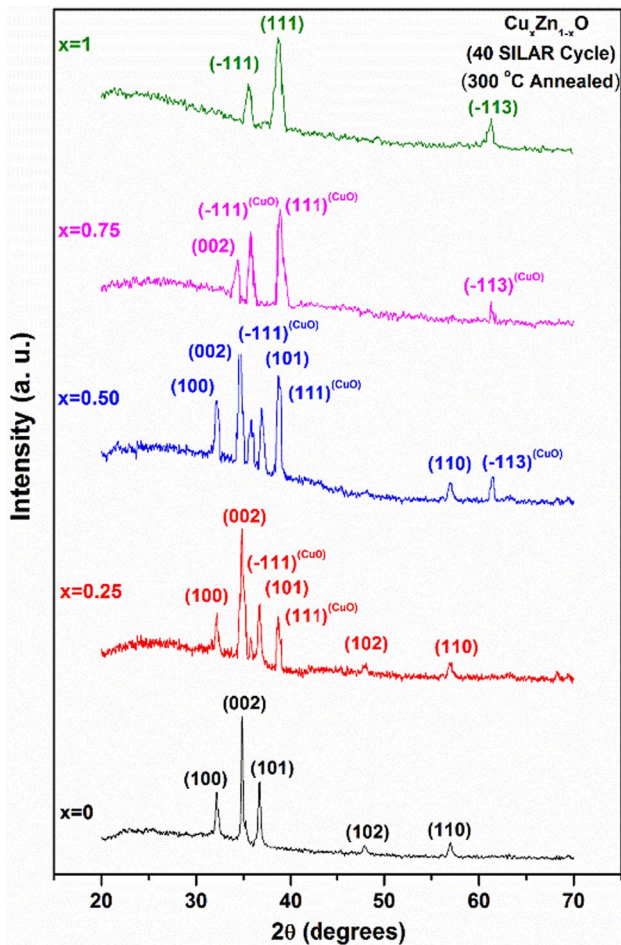


Fig. 1 XRD patterns of $Zn_{1-x}Cu_xO$ sensors, S0 (black), S1 (red), S2 (blue), S3 (pink) and S4 (green). (Color figure online)

(101), (102) and (110) diffraction peaks (JPCDS Card No: 36-1451) [23]. The pure CuO nanostructure ($x = 1$) had monoclinic phase with (-111), (111) and (-113) diffraction peaks (JPCDS Card No: 80-1916) [24]. The pure ZnO and pure CuO nanostructures had a strong preferred orientation along the (002) plane and (111) plane, respectively. As seen in Fig. 1, the intensity of the characteristic peaks of ZnO nanostructure decreased and some peaks disappeared in high Cu concentrations, whereas the characteristic peaks of CuO nanostructure began to appear and the intensity of the peaks increased with increasing Cu concentration (x). Thus, the dominant crystal structure of $Zn_{1-x}Cu_xO$ nanostructures changed from hexagonal wurtzite to monoclinic with increasing Cu concentration (x) from 0 to 1. The crystal quality of the nanostructures deteriorated with increasing Cu concentration (x). This deterioration could be attributed to changes in the atomic environment due to the extrinsic doping (Cu) of ZnO nanostructures. The changes in the atomic environment were ascribed to the differences in ionic radii of Zn and Cu elements, the smaller ($Cu_{Zn}-O_4$) unit and the shorter $Cu_{Zn}-O$ bonds in $Zn_{1-x}Cu_xO$ nanostructures [25].

The surface morphology of the nanostructured sensor materials affects the electrical and gas sensing properties of the material. Thus, it is very crucial to characterize the surface morphology of the nanostructures. Figure 2 shows the SEM images of $Zn_{1-x}Cu_xO$ nanostructures. As seen in Fig. 2, all the nanostructures had a compact and dense surface morphology. The full coverage of $Zn_{1-x}Cu_xO$ nanostructures on the interdigitated Au electrodes was obtained by using SILAR method. As clearly seen in Fig. 2a, ZnO nanostructure ($x = 0$) had nanorod structure and localized clusters on the surface morphology. $Zn_{0.75}Cu_{0.25}O$ nanostructure had a dense, uniform and well-grown flower-like structure (Fig. 2b). The SEM image of $Zn_{0.50}Cu_{0.50}O$

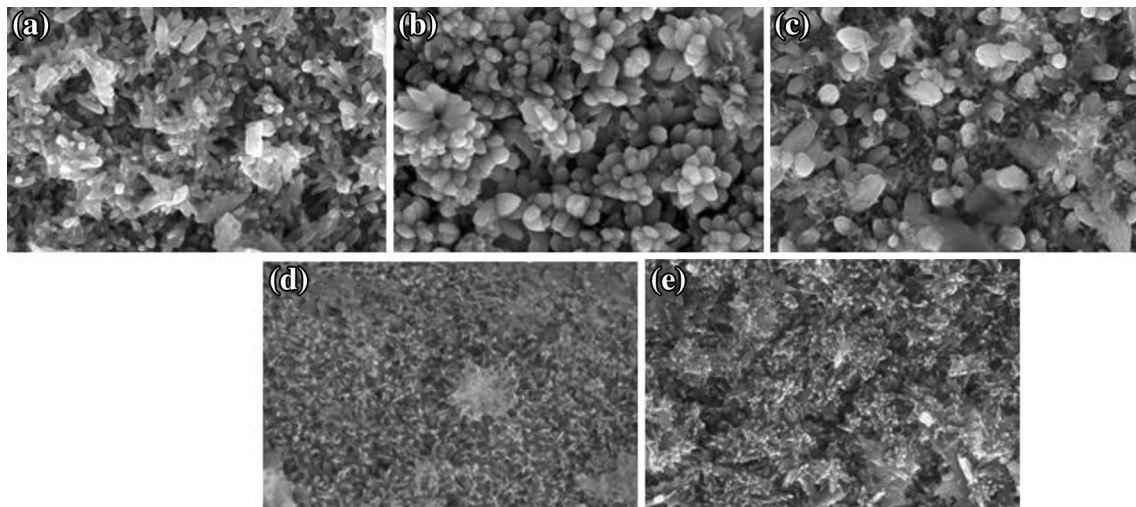


Fig. 2 SEM images of $Zn_{1-x}Cu_xO$ nanostructures, pure ZnO ($x = 0$) (a), $Zn_{0.75}Cu_{0.25}O$ (b), $Zn_{0.50}Cu_{0.50}O$ (c), $Zn_{0.25}Cu_{0.75}O$ (d), CuO (e)

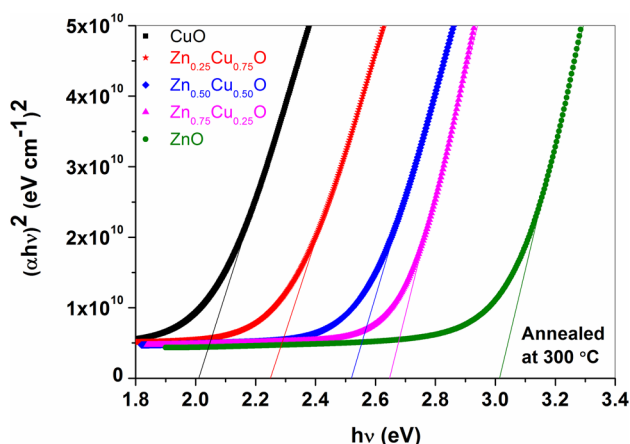


Fig. 3 $(\alpha h\nu)^2$ versus $(h\nu)$ plots of $\text{Zn}_{1-x}\text{Cu}_x\text{O}$ nanostructures

nanostructure (Fig. 2c) showed the distribution of the hexagonal grains with localized clusters and the CuO phase around the hexagonal grains. It was clearly seen that for $\text{Zn}_{0.25}\text{Cu}_{0.75}\text{O}$ and CuO nanostructures (Fig. 2d, e), the surfaces were densely covered with tiny grains compared to the others. SEM analyses showed that the surface morphologies of the $\text{Zn}_{1-x}\text{Cu}_x\text{O}$ nanostructures were altered by increasing concentration of Cu doping. The results were consistent with the literature [26].

The optical properties of $\text{Zn}_{1-x}\text{Cu}_x\text{O}$ nanostructures were determined by using the optical absorption measurements. The optical direct bandgap of the nanostructures can be determined by extrapolation of the linear region of $(\alpha h\nu)^2$ versus $(h\nu)$ plots using Tauc Eq. [27],

$$\alpha = \frac{A}{h}(h - E_g)^{1/2} \quad (2)$$

where, A is a constant, α is the absorption coefficient, E_g is the optical bandgap and $h\nu$ is a photon energy. Figure 3 shows $(\alpha h\nu)^2$ versus $(h\nu)$ plots of $\text{Zn}_{1-x}\text{Cu}_x\text{O}$ nanostructures. The bandgap values decreased from 3.01 to 2.01 eV with increasing Cu concentration (x). The decrease in bandgap value with increasing Cu concentration (x) could be attributed to a real bandgap change between ZnO and CuO due to, the formation of new recombination centers with lower emission energy in the nanostructures and the reduction in carrier concentration donated by interstitial zinc atoms or oxygen vacancies. The result was in agreement with the literature [27].

3.2 Gas sensing measurements of $\text{Zn}_{1-x}\text{Cu}_x\text{O}$ nanostructures (where, $x = 0, 0.25, 0.50, 0.75$, and 1)

As is well-known, the response of an MOS gas sensor is highly influenced by the operating temperature. For practical use, it is desirable to operate the devices at a lower

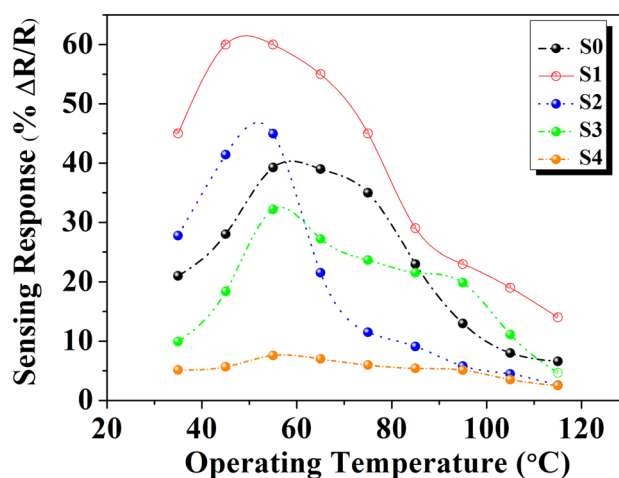


Fig. 4 The behavior of the sensor responses as a function of operating temperature. (Color figure online)

temperature [28, 29]. In order to explore the relationship between gas response and operating temperature, the sensors were tested for 25 ppm NO gas at different operating temperatures from 35 to 115 °C. Figure 4 shows the behavior of the sensor responses as a function of operating temperature.

The non-monotonic relationship between gas response and the temperature was observed at working temperature ranges, suggesting that 55 °C was the optimal operating temperatures for all the sensors. The sensing responses of S0, S1, S2, S3 and S4 were calculated to be 39, 60, 44, 32 and 8%, respectively. The maximum sensing response was obtained for $\text{Zn}_{0.75}\text{Cu}_{0.25}\text{O}$ (S1) sample. Figure 5 displays the dynamic gas measurements of the sensors for different gas concentrations from 50 ppb to 25 ppm at operating temperature of 55 °C. All the sensors experienced a rapid response when contacted with NO gas and then reached their stable response levels. As exposure to dry air, a very quick decrease of the sensor responses to their original states was observed. It was seen that the sensing response of all the sensors increased with increasing NO gas concentrations. Figure 6a and b shows the response of the sensors as a function of gas concentrations and the response of the sensors towards 50 ppb NO gas, respectively. The sensing response values of sensors towards 50 ppb NO gas were found to be 0.8, 8, 5, 3 and 0.1% for S0, S1, S2, S3 and S4 sensors, respectively. The response of the $\text{Zn}_{0.75}\text{Cu}_{0.25}\text{O}$ (S1) sensor towards 50 ppb of NO was approximately ten times higher than that of pure ZnO (S0). The results showed that S1 sensor exhibited the best gas sensing characteristics with respect to others. Sun et al. reported production of WO_3 and Cr_2O_3 powders for NO-selective gas sensor towards to low level (18 ppb) NO gas [30]. Mondal et al. examined YSZ electrolyte with WO_3 sensing material with Pt-zeolite/Pt as the reference electrode as and they showed that a catalytic filter

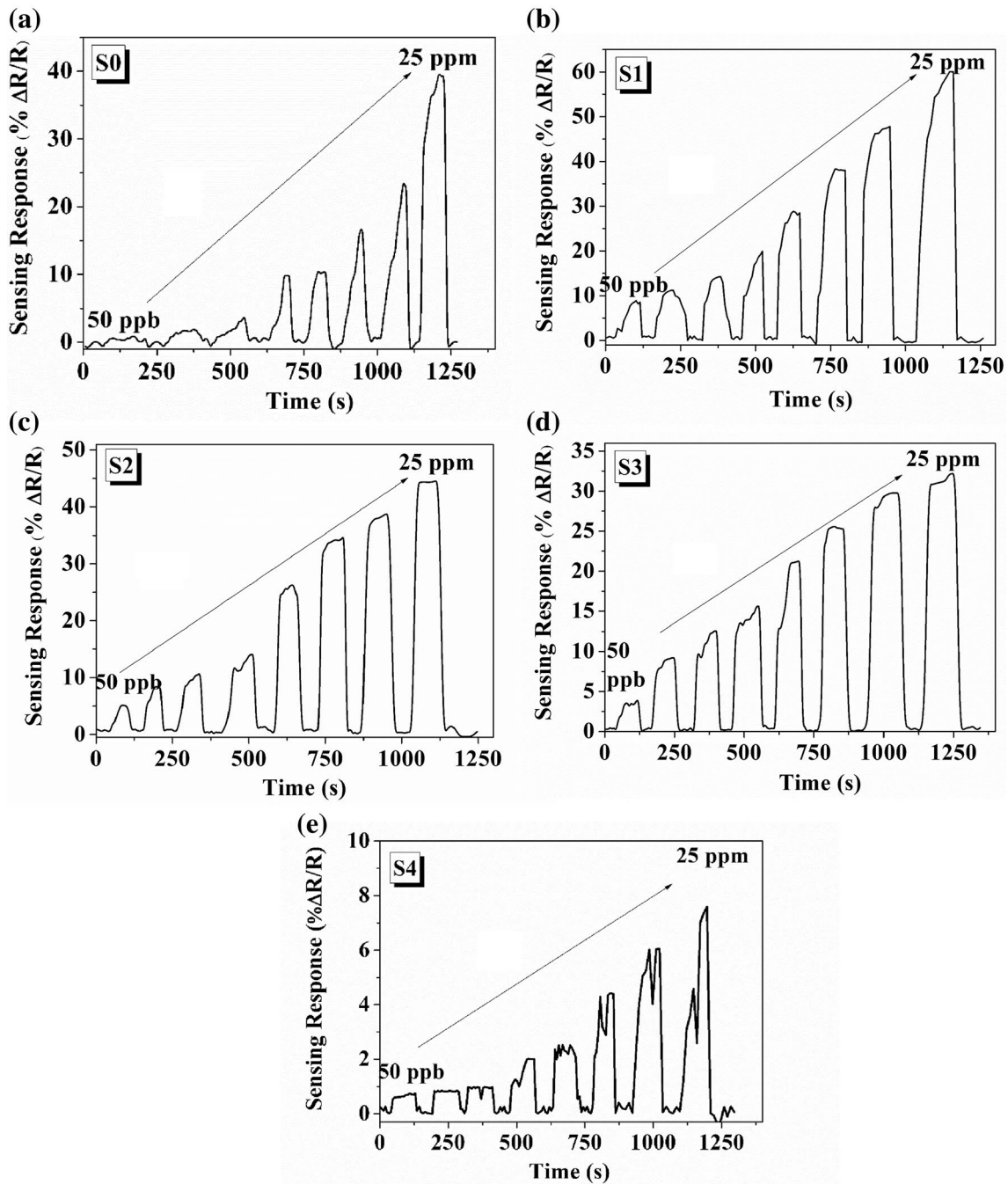


Fig. 5 The dynamic gas measurements of the sensors for different NO gas concentrations from 50 ppb to 25 ppm at 55 °C

allowed the cancellation of interferences due to oxidizable gases. They obtained acceptable responses towards 8 ppb NO gas [31].

Figure 7 shows the response and recovery times of the sensors towards various concentration of NO gas (50 ppb–25 ppm) at operating temperature of 55 °C. The response and recovery times decreased with increasing gas concentrations. The response and recovery times of the sensors towards NO gas at 55 °C were found to be 15–70 and

8–29 s at 50 ppb and 25 ppm gas concentration. The minimum response (15 s) and recovery (8 s) times were obtained for the S1 sensor. The fast response and recovery times are desirable for gas sensors [32, 33].

The sensing mechanism of resistive gas sensors based on n-type MOS is essentially considered from the electrical resistance change owing to an interaction between the adsorbed oxygen ion and target gases. When the sensing surface exposed the air, the adsorption of oxygen and formation of adsorbed

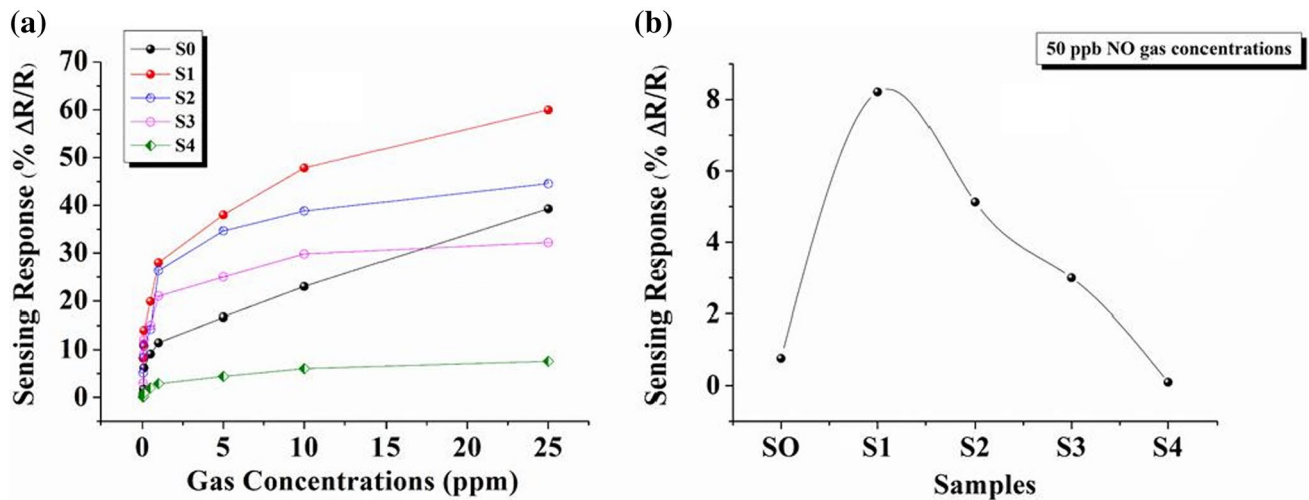


Fig. 6 The response of the sensors as a function of gas concentrations (a) and the response of the sensors towards 50 ppb NO gas (b)

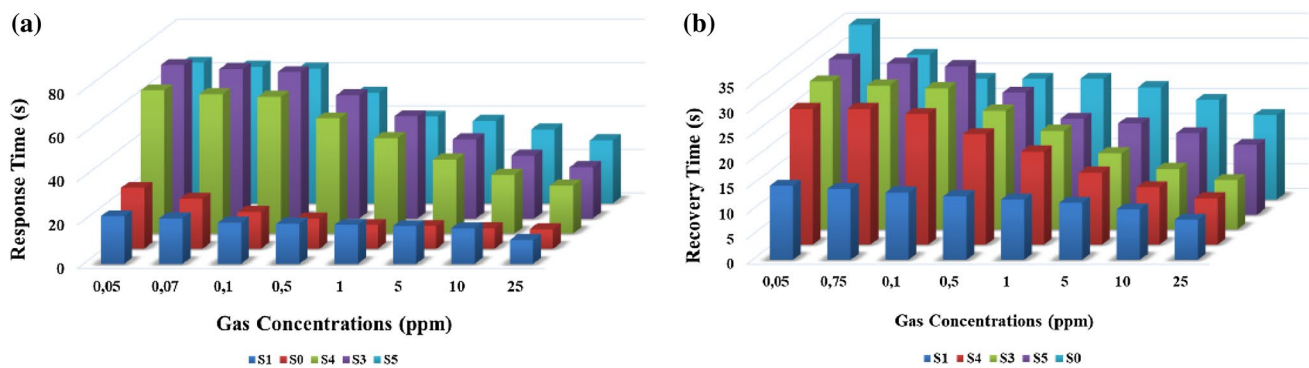
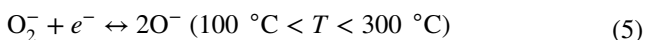


Fig. 7 The response **a** and recovery times **b** of the sensors towards various concentration of NO gas (50 ppb–25 ppm) at operating temperature of 55 °C. (Color figure online)

molecular/atomic oxygen ions such as O_2^- , O^- , O^{2-} are the essential mechanism, which takes place on surfaces of MOS gas sensors [32]. Then, depletion layers are formed on the surface regions, causing an increase in resistance of the oxide by the following formula [34]:



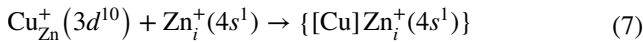
The reaction between the electron and the chemisorbed oxygen results in a decrease in the electron concentration at the surface of the sensor. When the sensing surface exposed to NO gas, the adsorption of NO causes electron transportation from sensing surface to NO due to high electrical attraction of the unpaired NO molecules, as shown in the following reaction [35];



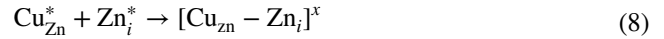
It is known that a depletion layer is generated in sensing material when it is exposed to an oxidizing gas such as O_2 , NO, etc. In the air, the conduction channel becomes narrower and a depletion layer is produced. The depletion layer thickness increases as the sensor are exposed to NO and the sensor resistance increases. Furthermore, Cu^+ acts as a catalyst that facilitates NO adsorption and desorption with the chemical reaction. The catalytic effect leads to a much narrower conduction channel in the sensing layer upon NO exposure which causes higher responses [32].

Generally, the response and selectivity are enhanced when noble metal catalysts are added on the metal oxide sensors due to catalytic effect [19]. Catalytic Cu is known as chemical sensitizer and electronic sensitizer, respectively. Cu can spill over the dissociated molecules to the metal oxide surface to activate the reaction with the chemisorbed oxygen species. For Cu-doped ZnO, the stability of the Coulomb forces of the interactions between the acceptor defects

(Cu⁺Zn) and intrinsic ZnO donors, namely, zinc interstitials or oxygen vacancies (Zn_i or V_O) can occur by the capture of an electron from the lattice. A model of an associate donor–acceptor for CuZn was proposed by West et al. [19];



In the Kröger–Vink notation,



The surface potential barrier for electrons in the conduction band can be increased by the created complex defects

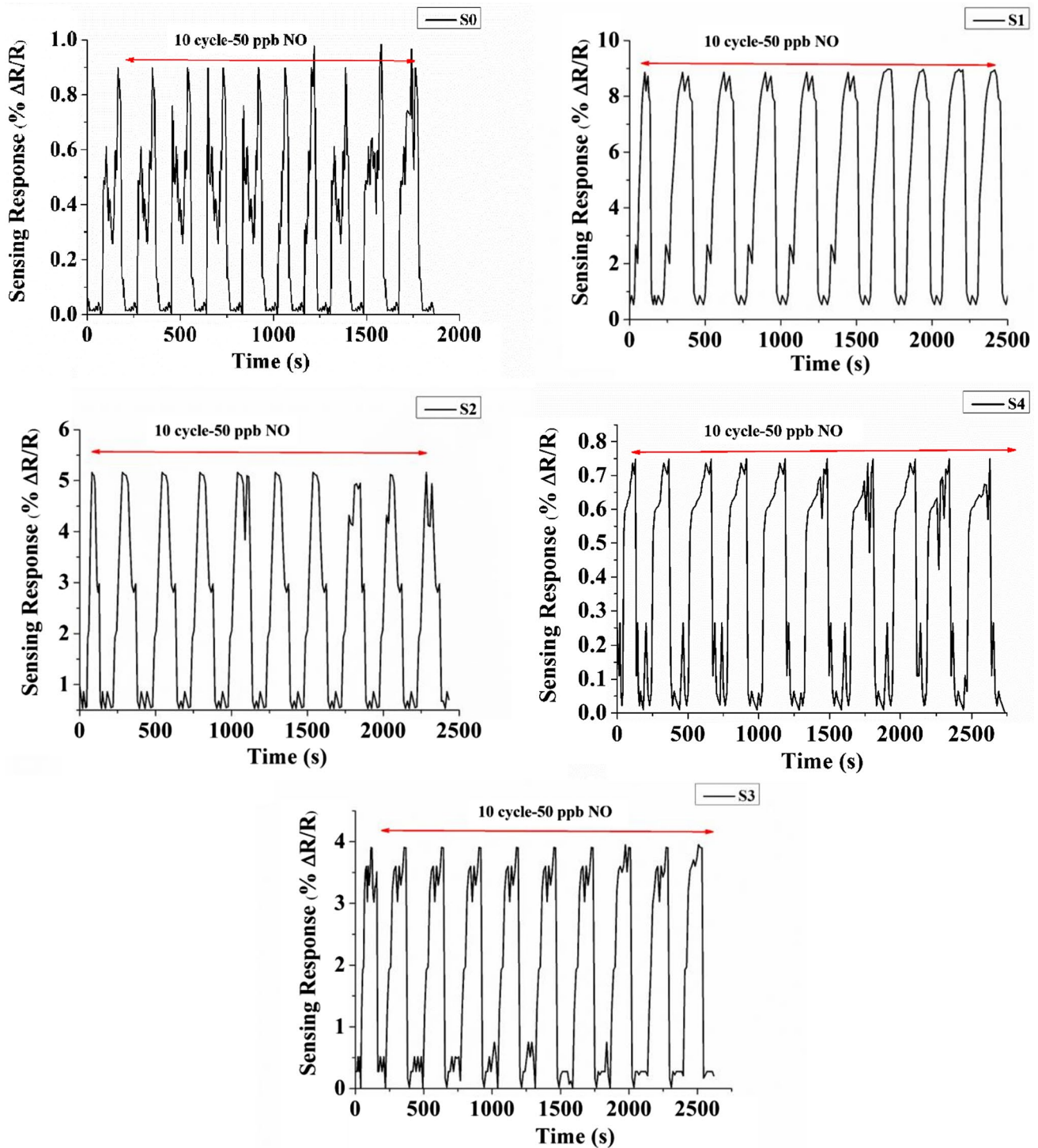


Fig. 8 The repeatability of the sensors exposed to 50 ppb NO gas

in Cu-doped ZnO. In general, the amount of adsorbed oxygen species on the surface would depend on the Cu atoms in the ZnO, which in turn would oxidize the exposed gas. Eventually, while the Cu concentration on the ZnO surface increases, it leads to the higher response due to the increase in the amount of adsorbed oxygen on the film surface [19]. In other words, the Cu atoms are weakly bonded to the oxygen atoms, and the resulting complex is readily dissociated at relatively low temperature and the oxygen atoms are produced. The created atoms migrate along the surface of the grains. This migration is induced by the catalyst atoms and is known as a spillover of the gas ions [19]. The oxygen atoms capture electrons from the surface layer and acceptor surface states are formed. As a result of this amount of Cu, doping would also be sufficient to promote the catalytic reaction effectively and the overall change in the resistance on the exposure of NO gas leading to an increase in the response. When the amount of Cu is less than the optimum, the surface dispersion may be poor and the response of the film is observed to be decreased since the amount may not be sufficient to promote the reaction more effectively [19].

Repeatability and stability are other crucial parameters, which need to be determined to ensure the long-term reliability of the sensor. Figure 8 shows the repeatability of sensors exposed to 50 ppb NO gas. The measurements were carried out for ten cycles. Stability refers to the capacity that a device has to give the same information under certain conditions, independently of the number of times this device has already been used. To evaluate the stability of these sensors, the responses were measured for 45 days. As shown in Fig. 9, the S1 sensor exhibited quite stable response at the 50 ppb NO gas concentration. It could be concluded that the stability of this material was good enough in long time detection of NO gas without any performance degradation in 45 days.

Selectivity of the sensor also plays a vital role in evaluating the efficiency of the gas sensor. The selectivity of the

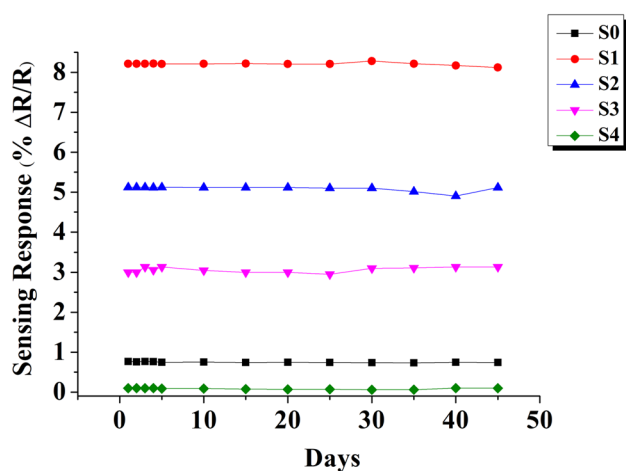


Fig. 9 The stability of the sensors measured for 45 days

sensor to gas molecules is greatly affected by the chemical composition of sensor materials as well as by the operating temperature of sensor. This allows us to propose the different chemical and physical nature of the sensor response in the case of each target gas which requires particular consideration [36]. Figure 10 indicates the selectivity of sensors exposed towards NO, CO, NH₃, H₂, CO₂, ethanol and acetone gases. The responses obtained towards CO₂, H₂, ethanol, and acetone gases were negligible, which could be attributed to the low operating temperature. In the literature, operating temperature of the sensors towards these gases is high [37–39]. Set et al. studied Co:ZnO nanorods as a H₂ gas sensor and they obtained maximum responses at operating temperature of 300 °C [41]. Liu et al. tested ZnO/SnO₂ spheres composite material as an ethanol gas sensor at operating temperature of 225 °C [38]. Wang et al. reported Mn and Cd doped ZnO nanomaterials as acetone ethanol gas sensors and the results showed that Mn doped ZnO exhibited a higher response to acetone than ethanol at operating temperature of 340 °C [39].

As seen in Fig. 10, the S1 sensor shows the maximum response towards NO gas. Although S1 sensor showed negligible responses towards H₂, CO₂, ethanol and acetone gases, it exhibited acceptable responses towards CO and NH₃ gases. To overcome the lack of selectivity towards CO and NH₃ gases, zeolite A filter layer was coated on the S1 sensor by using secondary growth method.

3.3 Gas sensing measurements of zeolite A coated Zn_{0.75}Cu_{0.25}O sensors

The overall results showed that Zn_{0.75}Cu_{0.25}O sensor (S1) exhibited the best gas sensing characteristics in terms of sensitivity, repeatability, stability, response and recovery times (Sect. 3.2). Therefore, Zn_{0.75}Cu_{0.25}O (S1) sensor was chosen to be modified with zeolites to increase sensor selectivity. Zeolite A film was coated as a filter on the S1 sensor for improvement of the sensor selectivity. In the first step, cubic zeolite A crystals (~100 nm) were synthesized and deposited on the Zn_{0.75}Cu_{0.25}O sensor by a spin coater. Then, the seed crystals deposited Zn_{0.75}Cu_{0.25}O sensor was grown hydrothermally. The XRD analysis showed that the synthesized zeolite A film was matched well with JPCDS Card No: 97-002-4901 (Supporting Information). The zeolite A film was pure and has no other phases. The cubic morphology of zeolite A crystal was not observed in SEM analysis (Supporting Information) since a compact and intergrown film with high degree of crystal contact was obtained by using secondary growth method [20, 40]. The thickness of the zeolite A coated Zn_{0.75}Cu_{0.25}O sensor was found to be 656.2 ± 12.7 nm from cross sectional SEM analysis. According to [Al₁₂Si₁₂O₄₈]8 stoichiometry of zeolite A (LTA) the ideal Si/Al ratio of the zeolite A is 1 [40]. SEM-EDX

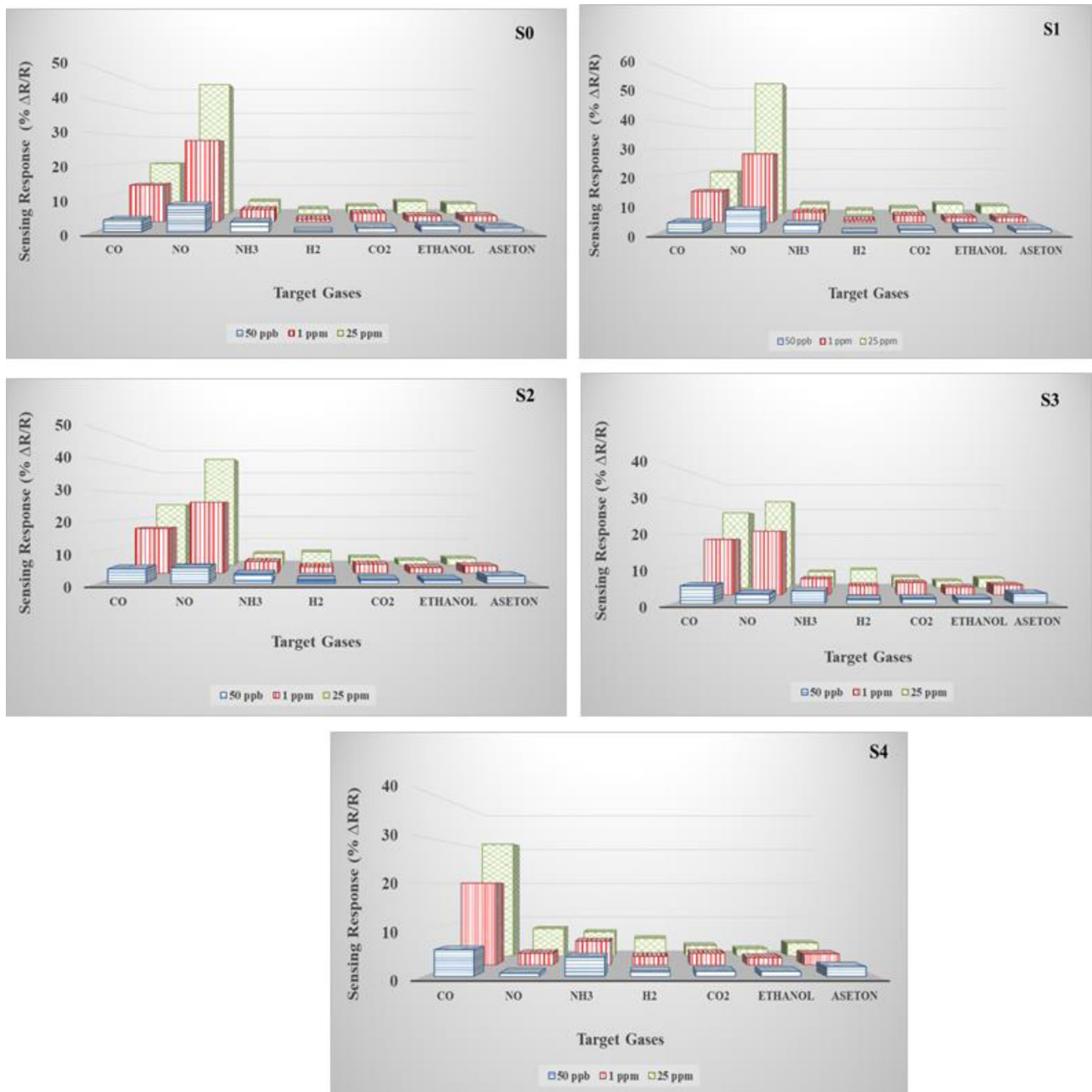


Fig. 10 The selectivity of the sensors exposed to NO, CO, NH₃, H₂, CO₂, ethanol and acetone gases. (Color figure online)

analysis revealed that the Si/Al ratio of the zeolite A coated Zn_{0.75}Cu_{0.25}O sensor was 1.3, which could be accepted in an experimental error [15].

The zeolite A coated S1 sensor was tested for NO, CO and NH₃ gases at the constant gas concentration of 20 ppb, as shown in Fig. 11. The sensor exhibited high selectivity towards NO gas and repelled the CO and NH₃ gases. Zeolites differ from other adsorbents in both their exceptionally large internal surface area and in their precisely defined pore diameter, which is of the order of molecular dimensions

[41]. In the current study, the operation temperature was room temperature for the zeolite A coated Zn_{0.75}Cu_{0.25}O sensor. At room temperature, the hydrophilic zeolite A possesses water adsorbed in the pores of zeolite and in the walls of intercrystalline spaces, hindering the passage of other molecules. Although NH₃ (NH₃ has kinetic diameters of 0.326 nm, smaller than the pore size of zeolite A of 0.41 nm) would be able to pass through the zeolite [42]. The water adsorbed in the pores of zeolite A at room temperature most likely hindered the passage of NH₃. Vilaseca et al. proved

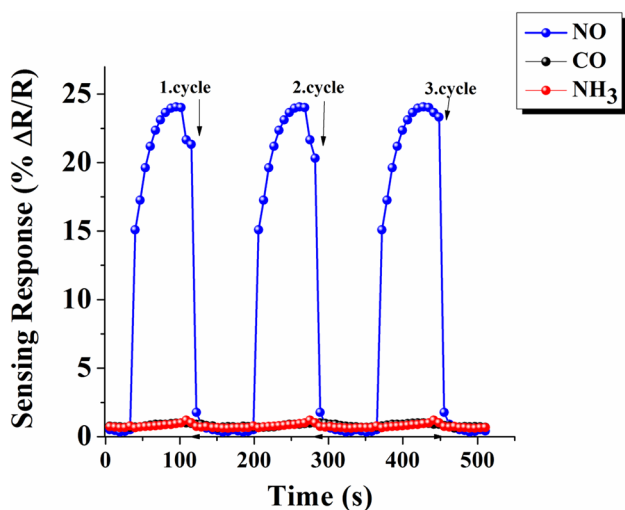


Fig. 11 The responses of the zeolite A coated $Zn_{0.75}Cu_{0.25}O$ (S1) sensor exposed to different target gases

that the filtering capacity of the LTA-type zeolite-modified sensors improves significantly when moisture-containing feeds are used (i.e., dry feed vs. 50% RH), by providing additional blocking molecules [43, 44]. In the case of CO sensing, the product gas was CO_2 which could also be adsorbed on the zeolite pores (water and CO_2 have kinetic diameters of 0.265 and 0.33 nm, respectively, smaller than the pore size of zeolite A of 0.41 nm) [44]. With both blocking effect of water and CO_2 on the hydrophilic zeolite A could contribute the observed changes in sensor selectivity. In the case of NO (NO has a kinetic diameter of 0.317 nm), although blocking the effect of water was expected since the operation temperature was room temperature, NO gas was passed through zeolite A pores (Fig. 11). It was proposed that the selectivity differences observed in gas sensing towards NH_3 , CO, and NO gases could be due to different diffusion rates and permeabilities of these gases through zeolite film [45].

The uncoated S1 sensor showed an acceptable response towards 50 ppb NO gas, while; zeolite A coated S1 sensor exhibited significant response towards 20 ppb NO gas. The detection limit of the NO gas was shifted from 50 to 20 ppb. The zeolite filter adsorbed the CO and NH_3 gases, while it allowed the NO gas to reach the sensor surface. Furthermore, the operation temperature of the zeolite A coated S1 sensor shifted from 55 °C to room temperature. The response of a sensor to a gas is affected by the diffusion of a vapor through the sensing material [15]. The zeolites have high surface area due to well-defined micropores within the zeolite crystals. It was proposed that, the sensor microstructure plays a key role in the kinetics of reactions taking place at the sensor surface; a more porous microstructure introduces a high area-to-volume ratio to the sensing element, as a result amplifying the concentration of surface-reactive sites that contribute to the

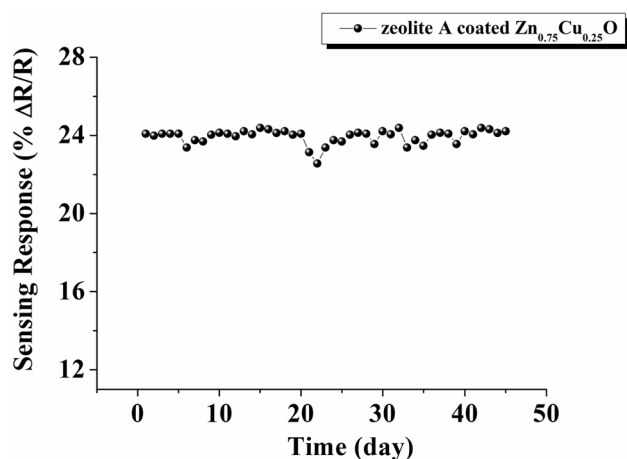


Fig. 12 The stability of the zeolite A coated $Zn_{0.75}Cu_{0.25}O$ (S1) sensor exposed to 20 ppb NO gas

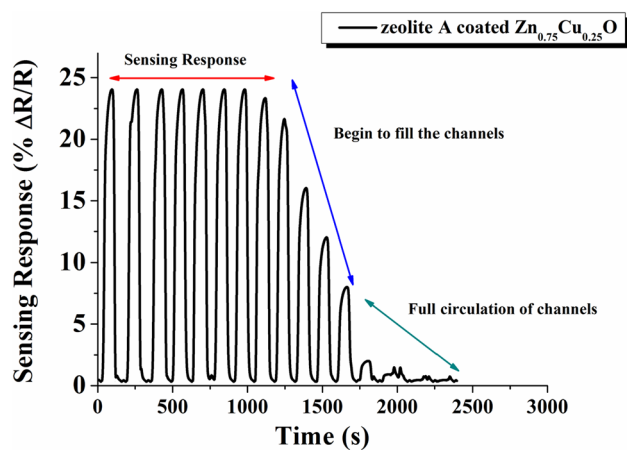


Fig. 13 The response of the zeolite A coated $Zn_{0.75}Cu_{0.25}O$ (S1) towards 20 ppb NO gas for different cycles

promotion of the overall conductivity of the sensing system [15]. The introduced high surface area enhanced the zeolite A coated $Zn_{0.75}Cu_{0.25}O$ sensor response with respect to the unmodified $Zn_{0.75}Cu_{0.25}O$ sensor. Furthermore, a more compact and intergrown zeolite layer was formed by applying secondary growth method when compared to screen printing, dip-coating and micro dropping techniques in the literature. It was suggested that the response of the sensor can be enhanced by the high degree of crystal continuity [45, 46]. Figure 12 depicts the stability of zeolite A coated S1 sensor. The sensor exposed to 20 ppb gas for 45 days. It can be seen from the results sensor showed good stability towards 20 ppb NO gas. The baseline response was obtained in each measurement.

However, this procedure has to face the problems of a limited applicability (the adsorbent material must be selective towards the desired molecules) and the need for

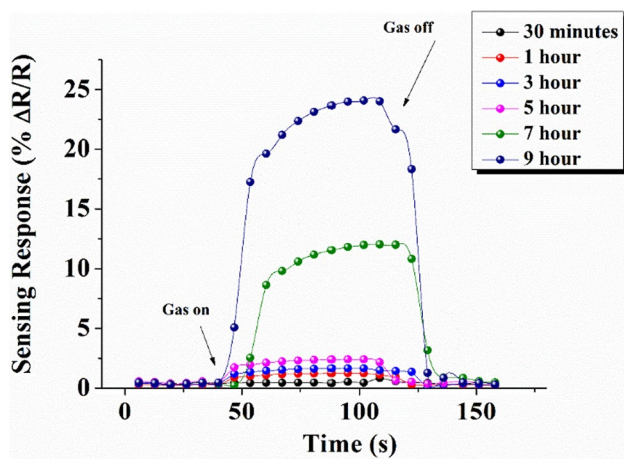


Fig. 14 The response of the zeolite A coated $\text{Zn}_{0.75}\text{Cu}_{0.25}\text{O}$ (S1) sensor as a function of regeneration time. (Color figure online)

periodic regeneration or replacement [47]. Figure 13 shows the short-term stability of the sensor towards 20 ppb NO gas. Sensitivity was stable throughout 8 cycles and began to fall after this point. After 12th cycle, no response was observed.

After the sensor was almost insensitive to NO gas, the measurements were repeated depending on the time for determination of the regeneration time. Figure 14 depicts the response of sensor as a function of regeneration time. There was no acceptable change after 5 h, the response obtained was at the same level. Then, regeneration process began after 7 h. The response was turned back to the initial value after 9 h. Under adsorption conditions, the target gas is adsorbed “irreversible” by the sensitive sensor layer since the adsorption rate is enhanced compared to the desorption rate, provoking the change of at least one material property due to gas accumulation [48]. In a short regeneration step under defined conditions, the formerly adsorbed gas molecules are released from the adsorbent and the adsorption capacity is recovered [49]. Commercial electronic nose instruments based on MOS technology always attach a new filter on the sensor for each new application [50]. The disposable filter must be changed for each new measurement session, which increases the cost. In our study, zeolite filter reached to the initial response after 9 h. Therefore, the need to change the filter for each measurement will be eliminated, which reduce costs and allow for the production of more suitable systems.

4 Conclusions

$\text{Zn}_{1-x}\text{Cu}_x\text{O}$ (where, $x=0, 0.25, 0.50, 0.75,$ and 1) sensors were grown by using SILAR method and their NO gas sensing properties were investigated comprehensively.

The response of the $\text{Zn}_{0.75}\text{Cu}_{0.25}\text{O}$ sensor to 50 ppb NO gas was 8% at a low operating temperature (55 °C). It was proposed that the catalytic effect of Cu, the concentration of Cu doping, and also the morphology of thin films affected the response of sensors. To increase the selectivity, $\text{Zn}_{0.75}\text{Cu}_{0.25}\text{O}$ sensor was coated with zeolite A film by using secondary growth method. The response and selectivity of zeolite A coated $\text{Zn}_{0.75}\text{Cu}_{0.25}\text{O}$ sensor towards NO gas was enhanced significantly. Furthermore, the detection limit of the NO gas was shifted from 50 to 20 ppb and the operation temperature of the sensor shifted to room temperature by coating intergrown zeolite A on the sensor element. The response of the zeolite A coated $\text{Zn}_{0.75}\text{Cu}_{0.25}\text{O}$ sensor towards 20 ppb NO gas was 25% at room temperature. The zeolite A filter reached to initial response after 9 h, which eliminates the need to change the filter for each measurement increasing the operation cost of the sensors. Modifying MOS sensors with intergrown zeolites will reduce costs and allow for the production of more suitable systems. The system shows the promise of electronic noses based on MOS technology.

Acknowledgements This work was supported by TUBITAK with Project No: 115M658 and Gazi University Scientific Research Fund Project No: 05/2016-21.

References

1. A. Mirzaei, S. Park, H. Kheel, G.-J. Sun, S. Lee, C. Lee, *Ceram. Intern.* **42**(5), 6187–6197 (2016)
2. Y. Li, D. Deng, X. Xing, N. Chen, X. Liu, X. Xiao, Y. Wang, *Sens. Actuators* **237**, 133–141 (2016)
3. E. Comini, *Mater. Today* **19**(10), 559–567 (2016)
4. Y. Li, J.-C. Liu, X.-X. Lian, T. Lü, F.-X. Zhao, *Trans. Nonferrous Met. Soc. China* **25**, 3657–3663 (2015)
5. M. Hjiri, L. El Mir, S.G. Leonardi, A. Pistone, L. Mavilia, G. Neri, *Sens. Actuators B* **196**, 413–420 (2014)
6. H. Gómez-Pozos, E.J.L. Arredondo, A.M. Álvarez, R. Biswal, Y. Kudriavtsev, J.V. Pérez, Y.L. Casallas-Moreno, M.L.O. Amador, *Materials* **9**, 87 (2016). doi:10.3390/ma9020087
7. L. Chow, O. Lupan, G. Chai, H. Khallaf, L.K. Ono, B.R. Cuenya, I.M. Tiginyanu, V.V. Ursaki, V. Sonté, A. Schulte, *Sens. Actuators A* **189**, 399–408 (2013)
8. X. Liu, S. Cheng, H. Liu, S. Hu, D. Zhang, H. Ning, *Sensors* **12**, 9635–9665 (2012)
9. J.N. Zemel, *Thin Solid Films* **163**, 189–202 (1988)
10. C.O. Park, S.A. Akbar, J. Hwang, *Mater. Chem. Phys.* **75**, 56–60 (2002)
11. M. Vilaseca, J. Coronas, A. Cirera, A. Cornet, J.R. Morante, J. Santamaria, *Sens. Actuators B* **124**, 99–110 (2007)
12. D.J. Wales, J. Grand, V.P. Ting, R.D. Burke, K.J. Edler, C.R. Bowen, S. Mintova, A.D. Burrows, *Chem. Soc. Rev.* **44**, 4290–4321 (2015)
13. G. Zhang, M. Liu, *Sens. Actuator B* **69**, 144–152 (2000)
14. S. Shinohara, Y. Chiyomaru, F. Sassa, C. Liu, K. Hayashi, *Sensors* **16**, 5–10 (2016)
15. P.T. Hernandez, S.M.V. Hailes, I.P. Parkin, *Sens. Actuators* **242**, 1281–1295 (2017)

16. S.N. Talapaneni, J. Grand, S. Thomas, H.A. Ahmed, S. Mintova, *Mater. Des.* **99**, 574–580 (2016)
17. M.M. Momeni, A.A. Mozafari, *J. Mater. Sci. Mater. Electron.* **27**(10), 10658–10666 (2016)
18. H.D. Dhaygude, S.K. Shinde, N.B. Velhal, M.V. Takale, V.J. Fulari, *Mater. Res. Expr.* **3**, 086402 (2016)
19. T. Çorlu, I. Karaduman, M.A. Yildirim, A. Ateş, S. Acar, *J. Electron. Mater.* **46**(7), 3995–4002 (2017)
20. S. Mintova, S. Mo, T. Bein, *Chem. Mater.* **13**, 901–905 (2001)
21. I. Karaduman, O. Barin, D.E. Yıldız, S. Acar, *J. Appl. Phys.* **118**, 174501 (2015)
22. I. Karaduman, E. Er, H. Çelikkan, N. Erk, S. Acar, *J. Alloy. Compd.* **722**, 569–578 (2017)
23. M.A. Yildırım, S.T. Yildırım, A. Ateş, *J. Alloys Compd.* **701**, 37–42 (2017)
24. Y. Caglar, D.D. Oral, M. Caglar, S. Ilcan, M.A. Thomas, K. Wu, Z. Sun, J. Cui, *Thin Solid Films* **520**, 6642–6647 (2012)
25. N.L. Tarwal, A.R. Patil, N.S. Harale, A.V. Rajgure, S.S. Suryavanshi, W.R. Bae, P.S. Patil, J.H. Kim, J.H. Jang, *J. Alloys Compd.* **598**, 282–288 (2014)
26. Z. Zhang, J.B. Yi, J. Ding, L.M. Wong, H.L. Seng, S.J. Wang, J.G. Tao, G.P. Li, G.Z. Xing, T.C. Sum, C.H. Alfred Huan, T. Wu, *J. Phys. Chem. C* **112**, 9579–9585 (2008)
27. Z.B. Bahsi, A.Y. Oral, *Opt. Mater.* **29**, 672–678 (2007)
28. C. Feng, C. Wang, P. Cheng, X. Li, B. Wang, Y. Guan, J. Ma, H. Zhang, Y. Sun, P. Sun, J. Zheng, G. Lu, *Sens. Actuators* **221**, 434–442 (2015)
29. C. Zhao, J. Fu, Z. Zhang, E. Xie, *RSC Adv.* **3**, 4018–4023 (2013)
30. C. Sun, G. Maduraiveeran, P. Dutta, *Sens. Actuators B* **186**, 117–125 (2013)
31. S. Mondal, P.K. Dutta, G.W. Hunter, B.J. Ward, D. Laskowski, R.A. Dweik, *Sens. Actuators B* **158**, 292–298 (2011)
32. L.-Y. Hong, H.-W. Ke, C.-E. Tsai, H.-N. Lin, *Mater. Lett.* **185**, 243–246 (2016)
33. J.G. Monroy, J. Gonzalez-Jimenez, J.L. Blanco, *Sensors* **12**, 13664–13680 (2012)
34. X. Liu, B. Cheng, J. Hu, H. Qin, M. Jiang, *Sens. Actuators B* **133**, 340–344 (2008)
35. W.-T. Koo, S.-J. Choi, N.-H. Kim, J.-S. Jang, I.-D. Kim, *Sens. Actuators B* **223**, 301–310 (2016)
36. V. Krivetskiy, A. Ponzoni, E. Comini, S. Badalyan, M. Rummyantseva, A. Gaskova, *Electroanalysis* **22**(23), 2809–2816 (2010)
37. D. Sett, D. Basak, *Sens. Actuators B* **243**, 475–483 (2017)
38. J. Liu, T. Wang, B. Wang, P. Sun, Q. Yang, X. Liang, H. Song, Gi Lu, *Sens. Actuators B* **245**, 551–559 (2017)
39. J. Wang, J. Yang, N. Han, X. Zhou, S. Gong, J. Yang, P. Hu, Y. Chen, *Mater. Des.* **121**, 69–76 (2017)
40. R. Xu, W. Pang, J. Yu, Q. Huo, J. Chen, (Wiley, Singapore, 2007)
41. K. Alberti, F. Fetting, *Sens. Actuators B* **21**(1), 39–50 (1994)
42. X. Xu, J. Wang, Y. Long, *Sensors* **6**, 1751–1764 (2006)
43. M. Vilaseca, J. Coronas, A. Cirera, A. Cornet, J.R. Morante, J. Santamaria, *Catal. Today* **82**, 179–185 (2003)
44. M. Vilaseca, J. Coronas, A. Cirera, A. Cornet, J.R. Morante, J. Santamaria, *Sens. Actuators B* **133**, 435–441 (2008)
45. W.L. Rauch, M. Liu, *J. Mater. Sci.* **38**, 4307–4317 (2003)
46. A. Zampieri, A. Dubbe, W. Schwieger, A. Avhale, R. Moos, *Microporous Mesoporous Mater.* **111**, 530–535 (2008)
47. A. Groß, G. Beulertz, I. Marr, D.J. Kubinski, J.H. Visser, R. Moos, *Sensors* **12**, 2831–2850 (2012)
48. F.I. Khan, A.K. Ghoshal, *J. Loss Prev. Process Ind.* **13**, 527–545 (2000)
49. E. Liu, B. Sarkar, Z. Chen, R. Naidu, *Microporous Mesoporous Mater.* **225**, 450–455 (2016)
50. WEB (2017) <http://www.niox.com/en/about-niox-products/NIOX-MINO/>. Accessed 21 Jul 2017